Individual-based model for quorum sensing with background flow

Hannes Uecker[*], Johannes Müller[†], Burkhard A. Hense[‡]

April 11, 2014

Abstract

Quorum sensing is a wide-spread mode of cell-cell communication among bacteria in which cells release a signalling substance at a low rate. The concentration of this substance allows the bacteria to gain information about population size or spatial confinement. We consider a model for N cells which communicate with each other via a signalling substance in a diffusive medium with a background flow. The model consists of an initial boundary value problem for a parabolic PDE describing the exterior concentration u of the signalling substance, coupled with N ODEs for the masses a_i of the substance within each cell. The cells are balls of radius R in $\mathbb{R}^3$, and under some scaling assumptions we formally derive an effective system of N ODEs describing the behaviour of the cells. The reduced system is then used to study the effect of flow on communication in general, and in particular for a number of geometric configurations.

Keywords: Quorum sensing, parabolic PDE, drift, dimension reduction.

1 Introduction

Communication between bacteria is a rather common phenomenon [23]. The most prominent example is quorum sensing [22]: by measuring the concentration of certain signals that are released by all cells at a low, constitutive level, a given bacterium is able to measure the population density around its location. This explains the name, as the cells are able to decide if a certain population size, the quorum, is reached. The signalling substance is relatively cheap to produce and serves as a proxy to decide if it pays to release e.g. exoenzymes. If the diffusive space is large, and only few bacteria also produce exoenzymes, it will not pay to fabricate these relatively expensive molecules. They simply diffuse away. If, however, many other cells nearby also start to generate these exoenzymes, then the concentration may reach levels such that it becomes efficient to release them. Often (but not always) quorum sensing is used to induce a synchronized action in a population that only pays if a large number of cells perform this action at the same time. In [18] it is recognized that not only a high population density but also confined space leads to a situation where the excretion of exoenzymes is beneficial: quorum sensing becomes "diffusion sensing", the bacteria test if substances do or do not diffuse away as a consequence of the geometry. Hense et al. [11] unified these two interpretations in the term "efficiency sensing", as ultimately it is only important if it pays to perform a certain action. It does not matter if this is the case as a quorum is reached, or because the diffusible space is restricted. In any case, if the concentration of the signalling substance exceeds a certain threshold, the bacteria change their life style. The resulting phenotype can be very different: not only exoenzyme production, but

[*]Institut für Mathematik, Universität Oldenburg, D-26111 Oldenburg, hannes.uecker@uni-oldenburg.de

[†]Centre for Mathematical Sciences, Technische Universität München, D-85748 Garching/Munich, johannes.mueller@mytum.de

[‡]Helmholtz Center Munich, Institut für Biomathematik und Biometrie, Helmholtzzentrum München, D-85764 Neuherberg, burkhard.hense@helmholtz-muenchen.de

also biofilm formation, swarming, or becoming virulent is under the control of quorum sensing for some bacterial species [23].

Quorum sensing gains increasing interest as a promising treatment target e.g. for pathogenic bacteria [19], requiring an adequate interpretation of its function. As described above, the interpretation of quorum sensing strongly depends on the spatial properties of the environment: a confined geometry and a batch culture may lead to completely different ideas about the purposes of quorum sensing. Most experiments, thought experiments, mathematical experiments, as well as biological experiments, take place in batch cultures, or stagnant water. However, most bacteria live – at least temporarily – in running water and lotic habitats. Experiments modelling runnels [17], or using microfluid devices [14] focus on the effect of flow (see also the review [12] and citations therein). Mathematical models that take into account flow are described e.g. in [21, 8], or the book of Eberl et al. [6]. These models, however, are often based on the Navier-Stokes equations, focus rather on biofilm formation than on cell-cell communication, and often are complex. They are quite realistic in that they take into account a lot of effects as the influence of the bacterial growth on the flow itself, but they cannot be treated analytically anymore. Another draw-back of these models is the fact that they mostly address the population density in the sense of classical reaction-diffusion-advection equations, and that they do not allow to reveal the dynamics of single cells and the interdependence of this dynamics via communication. An exception are models that are at least partially based on single cells, e.g. [1, 4]. These models are either still rather complex and do not target on analytic insight but on numerical simulations, or – in the other extreme – simple stochastic particle models and cellular automata that are used to focus on concepts and not on quantitative results.

In the present work, our interest is at an intermediate scale of complexity. Our model describes cells with fixed location in a laminar flow with constant velocity. The time evolution of the internal state of the cells is formulated by ODEs that couple via an outer field of signalling substances. The dynamics of the outer field is governed by a diffusion-advection equation. Even this simple model cannot be handled directly. In particular, the solution of the PDE for the outer field is rather involved, both analytically and numerically. Therefore we adapt the approximation techniques developed in [15, 16] to approximate the outer field by singularity solutions and thus reduce the system to a much simpler system of coupled ODEs. Additionally to the full space geometry we also consider cells in a confined space like a tube. The model thus allows to address the dynamics of single cells localized in a three dimensional space, and the intercellular communication, in a quantitative way, and some general rules of the influence of flow on cell-cell communication can be derived.

2 The model

In [16] we studied a model for communication of bacteria in a diffusive medium via a signalling substance produced by the cells. We briefly describe the model and extend it to allow for an external laminar background flow.

We consider N ball-shaped cells centered around $x_1, \cdots, x_N$. All cells have radius R, s.t. they cover the regions $\Omega_i = \{\|x - x_i\| \leq R\}$. The total mass (not concentration) of signalling substance within cell i at time t is denoted by $a_i(t)$, the concentration of signalling substance outside of the cells at location $x \in \Omega = \mathbb{R}^3 \setminus (\cup_{i=1}^N \Omega_i)$ and time t by $u(x,t)$. The dynamics of the model consists of three parts: (1) the production and degradation within the cells, (2) the diffusion/convection outside of the cells, and (3) the communication between inside and outside. (1) *Internal dynamics.* Following the usual approach [5, 16], we do not address any spatial structure within cells, but assume the substance to be homogeneously distributed. Furthermore, the regulatory network is collapsed into one ordinary differential equation, e.g. using time scale arguments. Although it is no problem to handle a system of ODE's here, for convenience we

treat the scalar case

$$a_i' = f(a_i).$$

The function f incorporates the production and internal degradation. Usually, signalling substance is produced at a constitutive rate α_0, and the production is enhanced by a positive feedback modelled by a Hill function with Hill coefficient n, threshold a_{thresh}, and maximal increase of the production rate β_0; additionally, there is a degradation with rate η. Thus, a minimal model for the internal regulatory pathway reads

$$f(a) = \alpha_0 + \frac{\beta_0 a^n}{a_{\text{thresh}}^n + a^n} - \eta a. \tag{1}$$

This model leads to bistablility in suitable parameter ranges: if the concentration of signalling substance is large enough, the Hill function indicates that the production term is increased, s.t. the concentration becomes even higher. Decisive for this scenario to happen is in particular the Hill coefficient. Experiments show that n is in the range between two and three [7]. We find later that diffusive transport dominates degradation, and thus here we set $\eta = 0$.
(2) *Diffusion-convection in the outer space.* First of all, the signaling substance is assumed to diffuse at linear rate D. Additional to [16] we now assume a laminar background flow $c \in \mathbb{R}^3$. The basic assumptions are that cells stay in place but are so small that they do not perturb the flow. Obviously this is a rather crude assumption, but appropriate if we think of small cells in a slow velocity field and not of large colonies and a fast flow. We obtain

$$u_t = D\Delta u - c^T \nabla u \text{ in } \Omega.$$

(3) *Boundary conditions and communication between inside and outside of the cells.* The flow of the diffusion-convection equation reads $j = -D\nabla u + cu$, s.t. $u_t = -\nabla \cdot j$ in Ω. If ν is the outer normal of Ω, the diffusion-convection flow j into cell i is given by $\nu^T j\big|_{\partial\Omega_i}$, and this must balance with terms $\tilde{j}$ describing the role of the cell. A natural assumption is the proportionality of $\tilde{j}$ to the outside concentration $u|_{\partial\Omega_i}$ and inside mass a_i. Later, we will rescale the radius R, and in order to minimize the effect of this rescaling, we also rescale the proportionality constants. The outflow part of $\tilde{j}$ scales with the surface of the cell, i.e. with R^2. To balance this dependency, we multiply the corresponding proportionality constant d_2 by R^{-2}. In consequence, $u|_{\partial\Omega_i}$ develops a pole of first order for $R \to 0$, and hence, we rescale the inflow proportionality constant d_1 by $1/R$. The boundary conditions of the PDE now read

$$\nu^T j\big|_{\partial\Omega_i} = \nu^T(-D\nabla u + cu)\big|_{\partial\Omega_i} \overset{!}{=} \frac{d_1 u}{R} - \frac{d_2 a_i}{R^2}\bigg|_{\partial\Omega_i},$$

and the net flow J_i into the cell i is the integral of $d_1 u/R - d_2 a_i/R^2$ over $\partial\Omega_i$, i.e.,

$$J_i = \int_{\partial\Omega_i} \left(\frac{d_1 u}{R} - \frac{d_2 a_i}{R^2}\right) do.$$

Altogether, after rearranging the boundary conditions, the extended model takes the form

$$u_t = D\Delta u - c^T \nabla u \text{ in } \Omega, \quad u(x,0) = u_0(x), \tag{2a}$$

$$B_i u = \frac{d_2}{R^2} a_i(t) \text{ on } \partial\Omega_i, \quad \text{where } B_i u := \left[\nu^T \left[D\nabla u - cu\right] + \frac{d_1 u}{R}\right]\bigg|_{\partial\Omega_i}, \tag{2b}$$

$$a_i' = f(a_i(t)) + \int_{\partial\Omega_i} \left(\frac{d_1 u}{R} - \frac{d_2 a_i(t)}{R^2}\right) do, \qquad a_i(0) = a_{i0}, \tag{2c}$$

see Fig. 1 for a sketch.

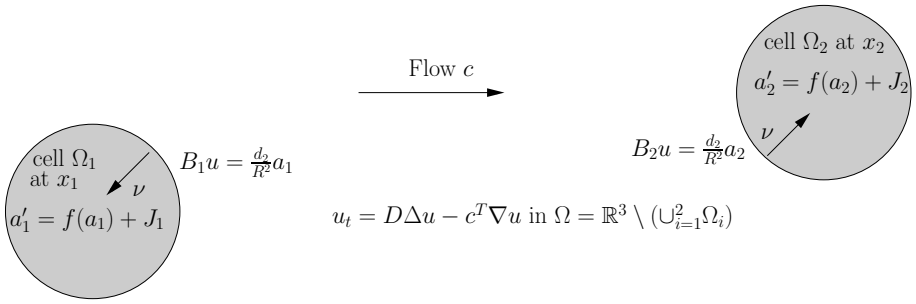

Figure 1: Sketch of the model setup for the case of two cells.

The goal is to derive effective (ODE) systems for the masses a_i in the limit of small cells $R \to 0$, and to compare the effect of diffusion with that of transport. We assume that the reaction resp. regulatory pathway of the cells has a slower time scale than the diffusive transport. This assumption is in line with observations and heuristic computations [9, 13, 20]. Proceeding in a similar way as in [16] we find the following result (see Appendix for the computations).

Result 1. *Model (2a)-(2c) can be well approximated by effective systems of the form*

$$a_i' = f(a_i) - M(1 + R\gamma|c|)a_i + R\frac{d_1 M}{D + d_1}\sum_{j\neq i}\frac{a_j}{|x_i - x_j|}\exp\left(\frac{c^T(x_i - x_j) - |c|\,|x_i - x_j|}{2D}\right), \quad (3)$$

where

$$M = \frac{4\pi D d_2}{d_1 + D} \quad \text{and} \quad \gamma = \frac{d_1}{2D(D + d_1)}. \quad (4)$$

The field u can then be reconstructed from

$$u(x,t) = \sum_{i=1}^{n}\Big[(\alpha_i(t) + R\beta_i(t))\psi_i(x - x_i) + R^2\theta_i(t)(c^T\nabla\psi)(x - x_i)\Big], \quad (5)$$

where

$$\begin{aligned}\alpha_i &= Ma_i, \qquad \beta_i = \frac{d_1|c|}{2D(D + d_1)}\alpha_i - \frac{d_1}{D + d_1}\sum_{i\neq j}\frac{\alpha_j}{|x_j - x_i|}e^{(c^T(x_j - x_i) - |x_j - x_i||c|)/(2D)},\\ \theta_i &= \frac{d_1}{2D(d_1 + 2D)}\alpha_i = \gamma\alpha_i,\end{aligned} \quad (6)$$

and where

$$\psi(x) = \frac{1}{4\pi D\,|x|}\exp\left(\frac{c^T x - |c|\,|x|}{2D}\right) \quad (7)$$

is the singularity solution of $Lu := D\Delta u - c\nabla u = 0$, i.e., $L\psi = \delta_0$.

Remark 2.1 By "well approximated" we mean the following. For a single cell we set $a_1 =: a$ and assume the compatibility condition $u_0(x) = Ma(0)\psi$. Then, for all $t_1 > 0$ there exist $R_0 > 0$ and $C > 0$ such that for all $0 < R < R_0$ the following holds: if (u, a) is the solution to (2), and

$\tilde{a}$ is the solution to (3) with initial condition $\tilde{a}(0) = a(0)$, then

$$\sup_{0\le t\le t_1} |a(t) - \tilde{a}(t)| \le CR\|a\|_{C^1}. \tag{8}$$

This result can be proven along the lines of the case $c = 0$ in [16, Theorem 4 and Corollary 5]; see also [16, Remark 2b)] for comments on the compatibility condition $u_0(x) = Ma(0)\psi$. In particular, the reconstructed u from (5) satisfies the the boundary conditions (2b) up to an $\mathcal{O}(R^0)$ error, and even though u satisfies the PDE (2a) only up to $\mathcal{O}(R^{-1})$, this turns out to be sufficient to prove (8) via approximation of (2) by a delay equation as an intermediate step. The asymptotic result (8) does not rely on a separation of time scales between the internal cell dynamics $a' = f(a)$ and diffusive transport. However, the error in (2a) is in fact $\mathcal{O}(R^{-1}a')$ and thus vanishes in the stationary case. From an application point of view, a slower time scale of the internal dynamics $a' = f(a)$ of the cells then reflects in well behaved constants R_0, t_1, C in (8), thus making the result applicable for finite $R > 0$.

For $n \ge 2$ cells, the results from [16] also transfer to $c \neq 0$ to give a result similar to (8), if one also assumes a certain scaling of cell distances. See [16, Theorem 10 and Corollary 11] for a precise formulation for $c = 0$.

However, the necessary steps to prove (8) and its analogon for $n \ge 2$ are quite technical and give little additional insight, compared to [16]. Therefore, in Appendix A we only give the formal derivation of (3), and below focus on the application of (3) to some example configurations. ⌋

Before we present quantitative simulations we state one important qualitative conclusion from the approximative equations.

Result 2. *In the range of validity of the model and the approximation, the flow always has a damping effect on the production of signalling substance of a single cell and the communication of cells.*

The first statement follows from the first order term $-RM\gamma|c|a_i$ in (3). This term indicates that the washout-effect always decreases the chance for a signal molecule once it left the cell where it has been produced to return to this cell. The second statement holds since $\left|\exp\left(\frac{c^T(x_i - x_j) - |c|\,|x_i - x_j|}{2D}\right)\right| \le 1$ for the velocity-depending weights in the communication terms in (3).

3 Simulation results

We assume that the cells live in three-dimensional space, releasing chemical signals, as described above. We compare the situation without flow ($c = 0$) and that with a moderate flow which is realistic for experiments in microfluid chambers. The device used in [14] has height 0.4 mm, width 3.8 mm, and length 17 mm; the flow is given by 2 ml/h resp. $|c| = |c_0| = 3.65 \cdot 10^{-4}$ (m/s). The parameters are close to those for the excretion of AHL by *Pseudonomas putida* (see e.g. [7]). We only adapt the coefficient modelling the influx rate constant into the cells in order to have a bistable situation for zero velocity; the situation at hand could be considered to describe a micro-colony. In this scenario, the results become more clear and pronounced. All parameters are summarized in Tab. 1.

We start off with one cell. As discussed above, the parameters are adapted in such a way that a single cell is supercritical (Fig. 2(a)). The efflux terms in the ODE $\dot{a} = f(a) - M(1 + R\gamma|c|)a$, modelling the washout-effect, become eventually dominant if the velocity is increased. At the same time, the outer field is deformed by the velocity field (Fig. 2(b),(c)). It is interesting to estimate the velocity at which the washout-effect breaks the positive feedback loop (Fig. 2(d)). We find that velocities around four times higher than that used in flow chamber experiments

Parameter	Value	Meaning and source
V_c	$1.96 \cdot 10^{-19}$ m^3/cell	volume per cell
R	$3.6 \cdot 10^{-7}$ m	radius iof a ball with volume V_c
D	$4.9 \cdot 10^{-10}$m^2/s	[12]
d_2	$0.008\ D/(4\,\pi\,R^2)$	[16]
d_1	$55\,d_2\,V_c/R$	[16]
α_0	$6.4 \cdot 10^{-23}$ mol/(s cell)	constitutive AHL expression, [7]
β_0	$6.4 \cdot 10^{-22}$ mol/(s cell)	activated AHL expression, [7]
c	$3.65 \cdot 10^{-4}$ m/s	assumption, see text and [14]
τ	70 n mol/l $\approx 1.37 \times 10^{-23}$ mol/cell	threshold, [7]
n	2.5	Hill-coefficient, [7]

Table 1: Parameters used in the simulations. The parameters are mostly taken from experiments with *Pseudonomas putida* [7], and from the paper [16]. The flow is adapted to micro-fluid device experiments [14]. For the derived parameters we find $M \approx 26.38$, $\gamma = d_1/(2D(D+d_1)) \approx 1.3{\cdot}10^8$, $R|c|\gamma = 0.01715$.

will lead to a breakdown: the internal state suddenly jumps from an activated level to a quiet level. This is due to a saddle-node bifurcation that destroys the activated branch of stationary points (see also Fig. 2 (a)).

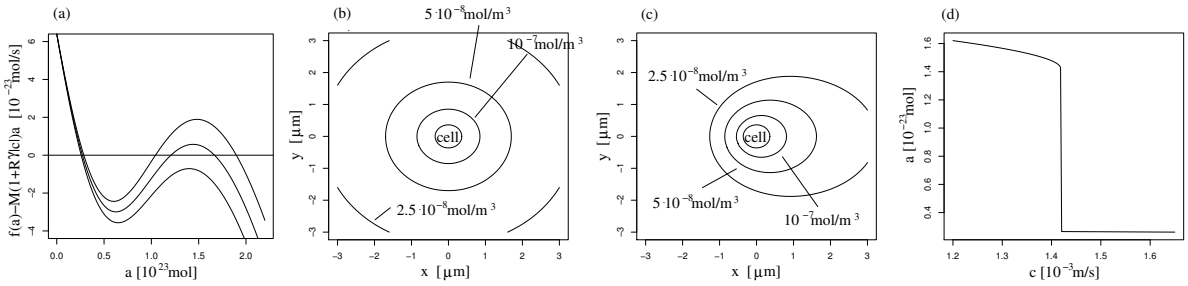

Figure 2: (a) Effective RHS for one cell, for $c = c_0 := 3.65\,10^{-4}$ m/s, $c = 3c_0$, $c = 5c_0$ (top down). (b),(c) u (level lines) reconstructed from fixed point for $c = 0$ and $c = 3.65\,10^{-4}$ m/s, other parameters as in Table 1. (d) dependence of the final cell state on flow velocity.

Next we investigate the influence of flow on the communication, i.e. on the interaction of two cells (or micro–colonies). We expect two competing effects: the washout effect, that we already found to be damping for one cell, and a downstream effect. Two geometrical settings are of particular interest as they represent two extreme cases: the cells may either be aligned or perpendicular with the direction of the flow. Figure 3 shows the results of such simulations. For $c = 0$, both geometrical settings are of course identical. In case of cells aligned with the flow, the downstream cell receives distinctively more signaling substance (see Fig. 3(b), (e)). If we investigate the break-down of the positive feedback caused by the flow (Fig. 3(c)), we recognize that there is almost no upstream communication: the velocity at which the positive feedback breaks down is very close to the critical velocity in the one-cell case. The downstream cell, however, is able to stay longer activated as the upstream cell. Even if the upstream cell is in the quiet state, the little additional amount of signalling substance washed to the downstream cell helps the latter to stay activated substantially longer. The perpendicular activation breaks down at a velocity between that of the upstream- and the downstream case (Fig. 3(f)). Obviously, reciprocal communication is longer possible perpendicular than upstream. However, in summary, all communication breaks down at rather small velocities due to the washout effect.

The last scenario models confined space. The intuitive idea is that a confined space does

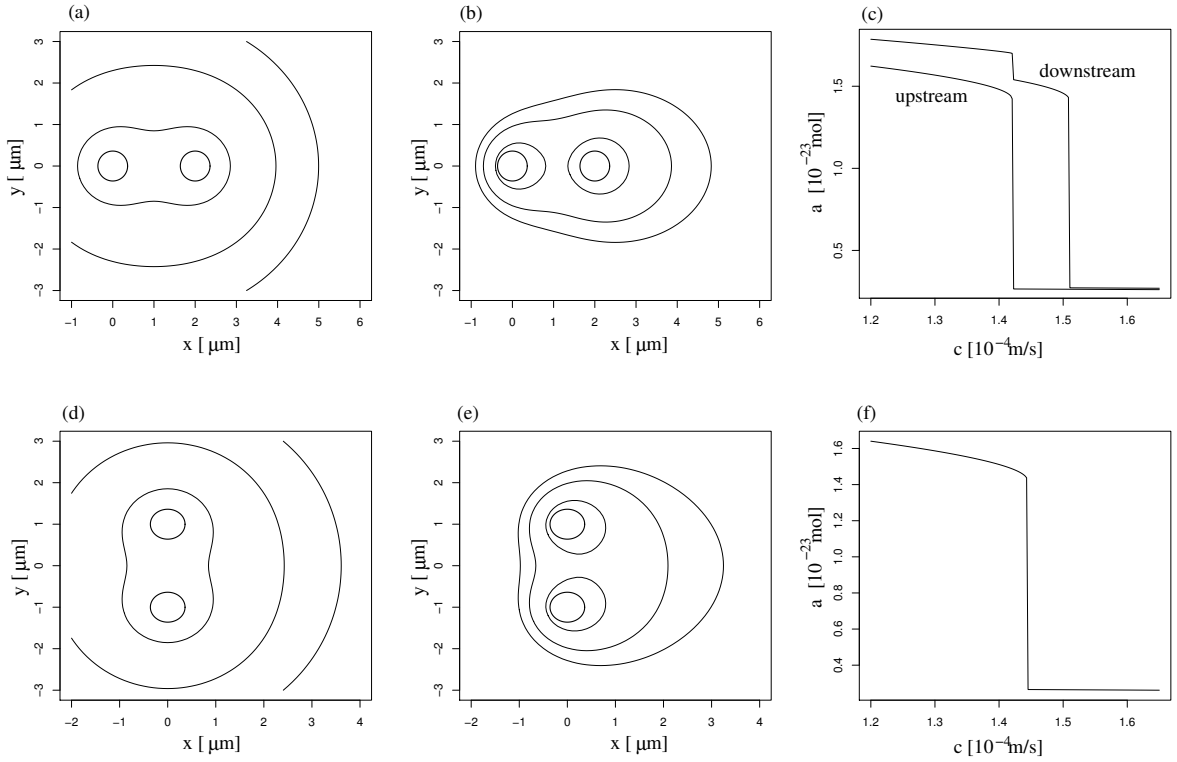

Figure 3: Two cells at a distance of 2 μm, parallel (a), (b), (c) and perpendicular (d), (e), (f) to the flow. c=0 in (a), (d), c=3.65 10^{-4} m/s in (b), (e); level lines are given at $2 \cdot 10^{-7}$, 10^{-7}, and $0.7 \cdot 10^{-7}$ mol/m^3. (c) and (f) show the internal state a_i of the cells. Note that in (d) the two states are identical for symmetry reasons. Parameters as in Table 1.

not allow the signalling substance to diffuse and in this way the downstream effect should be strengthened. The very simple scenario considered here consists of a tube with rectangular profile, a number of cells in the shape of half–spheres sitting on the inner surface of the tube, and a laminar constant flow directed along the symmetry axis of the tube, see Fig. 4. In particular we assume perfect slip boundary conditions. This assumption is wrong for any real application, but this simple setup can be treated via (3) by suitably introducing virtual cells, see §A.3 for details, and even in this simple setup we find several remarkable results.

Firstly, theory and simulations show that still the washout dominates the downstream effect. Figure 4(b1) shows the situation for 6 cells and a vanishing small flow ($c = 10^{-10}$ m/s), which we use to simulate the situation without flow ($c = 0$) only for technical reasons, i.e., to remove some formal divergence, see the comments before (20). Here, each of the cells is activated, with essentially $a_1 = a_6, a_2 = a_5, a_3 = a_4$ by symmetry, and the middle cells have the largest a. For $c = 3.65\ 10^{-5}$ m/s in (b2), the a_i increase with i, i.e., the last cell has the highest a_i. However, even for this small c, $\frac{1}{10}$ the reference c from Table 1 and Figures 2 and 3, this is the only activated cell, but at only about half of its state in (b1), while the 5 upstream cells are quiet. In (c1), for vanishing small c the middle cells are activated to a slightly larger state than in (b1). For $c = 3.65\ 10^{-5}$ m/s in (c2), now 5 cells downstream are activated, but for instance the 6th cell shows an almost identical behaviour to the 6th cell in (b2), indicating that upstream communivation from cells 7,8,9 and 10 to cell 6 is negligible. Thus, the second result is that also in the present geometry upstream communication is barely possible: A cell only recognizes the number of cells upstreams, and the number of cells downstream is barely important. We expect the result to be stable against more realistic geometries and flows, although quantitatively the

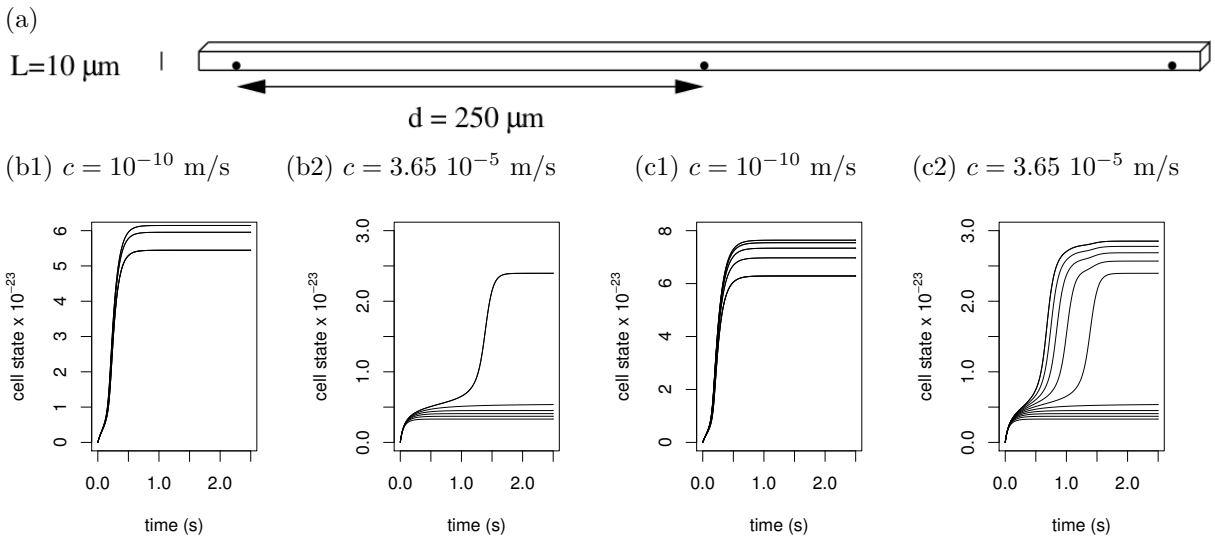

Figure 4: Communication in a tube. The geometry is indicated in (a): a rectangular tube of 10μm width and infinite length is considered. In distance of 250 μm, single cells (indicated by bullets) are located on the tube's inner surface. (b) dynamics of the internal states of six cells, for $c = 10^{-10}$m/s and $c = 3.65\ 10^{-5}$ m/s, starting with zero initial conditions for all cells. (c) Analogous to (b) for 10 cells.

model is rather sensitive with respect to, e.g., L. For instance, for ten cells with parameters as above but with $L < 6\mu$m all ten cells become activated while for $L > 14\mu$m all ten cells stay quiet.

4 Discussion

Intuitively, there are two counteracting effects of a laminar flow: the washout and the downstream effect. Signalling substance is washed away, and thus communication is interrupted. However, cells that are located downstream of other cells should receive more communication signals. Consider N cells aligned in a row, and no flow. Assume that this population just reaches its quorum. If a moderate flow is applied, we expect the first cells to become subcritical due to the washout effect. On the other hand, if without flow the population is just subcritical, we expect the last cells to become supercritial if a moderate flow is applied, due to the downstream effect. However, in our model we found that for the stationary state flow is always damping, i.e., the washout always out-competes the downstream effect. This even holds in a confined space like a tube, though downstream effects are longer visible as the signalling substance cannot diffuse away in the direction perpendicular to the tube walls.

These seemingly counter-intuitive results are based on the fact, that in a scenario without flow, the signalling substance is able to accumulate; only diffusive transport counteracts an unbounded accumulation. In a confined space like a tube this accumulation is even stronger than in the three dimensional space. In the long run, this increase leads to higher signal concentrations than the downstream effect is able to create, even if many cells are located upstream.

Our theoretical results are in line with experimental observations [14], where a microfluid device has been used to study the communication between colonies. It turned out that at no-flow conditions, the colonies have been activated much earlier than with flow, and that in the case with flow, a downstream effect has been barely recognizable. These findings indicate that for realistic settings that incorporate even an intermediate flow, quorum sensing is not able to create a population–wide communication, contrary to what batch culture experiments and mathematical models without flow state. An aspect that becomes more prominent in recent time

is that much of cell-cell communication happens in colonies and biofilms [10]. These habitats are protected against much of the surrounding flow by an extracellular matrix. Interestingly, a (partial) restriction of communication to single colonies fits to the prediction of theoretical evolution that fluctuation of (sub)populations through bottlenecks (as new emerging colonies) may evolutionary stabilize quorum sensing based cooperation against non-contributing cheater mutants [3]. Meyer et al. [14] thus speculated that between colonies rather competition than cooperation should be an evolutionary stable strategy. It is likely that often quorum sensing only is aimed at bacteria within the same colony or within a biofilm, and the signal is not meant to spread globally as the original interpretation as quorum sensing suggested. In this sense, quorum sensing is likely to be rather an intra-colony and short-range communication.

A The reduction

Here we give the calculations to approximate the coupled PDE–ODE systems (2) by ODE systems of the form (3). For simplicity we first consider only one cell. The generalization to $N \geq 2$ cells as in Result 1 then works rather naturally, and finally we explain how to treat the spatially confined case.

A.1 One cell

Consider a single cell, located in $x = 0$ with radius $R > 0$. In lowest order we let $u = \alpha\psi(x)$ with $\psi(x) = \dfrac{1}{4\pi D\,|x|}\exp\left(\dfrac{c^T x - |c|\,|x|}{2D}\right)$, cf. (7), and choose α such that the BC

$$Bu|_{|x|=R} = \left[\nu^T\left[D\nabla u - cu\right] + \frac{d_1}{R}u\right]|_{|x|=R} \stackrel{!}{=} \frac{d_2}{R^2}a \tag{9}$$

are satisfied to leading order. We have

$$\nabla\psi(x) = \frac{1}{4\pi\,D}\left(-\frac{x}{|x|^3} + \frac{c}{2D|x|} - \frac{x|c|}{2D|x|^2}\right)e^{(c^T x - |x||c|)/(2D)}.$$

Since $\nu = -x/|x|$, (9) thus yields

$$\frac{\alpha}{4\pi\,D}\left(\frac{D}{R^2} + D\frac{|c| - \frac{c^T x}{R}}{2DR} + \frac{c^T x}{R^2} + \frac{d_1}{R^2}\right)e^{(c^T x - R|c|)/(2D)} = \frac{d_2 a}{R^2}.$$

As $e^{(c^T x - |x||c|)/(2D)}\Big|_{|x|=R} = 1 + \mathcal{O}(R)$, we find in leading order ($\mathcal{O}(R^{-2})$)

$$\alpha = Ma \text{ with } M = \frac{4\pi D d_2}{D + d_1}, \tag{10}$$

independent of c.

Next, as $\int c^T x \mathrm{d}o = 0$,

$$\int_{|x|=R}\frac{\psi}{R}\mathrm{d}o = \frac{1}{4\pi\,D}\frac{1}{R^2}\int_{|x|=R}\mathrm{e}^{(c^T x - |x||c|)/(2D)}\mathrm{d}o = \frac{1}{D}\big[1 - R|c|/(2D) + \mathcal{O}(R^2)\big], \tag{11}$$

see however Remark A.2 for remarks on this expansion. Consequently, the already generalized

ansatz $u(x) = \alpha\psi(x) + \mathcal{O}(R^0)$ yields $\int_{|x|=R} \frac{d_1 u(x)}{R}\, do = \frac{d_1}{D}\alpha + \mathcal{O}(R)$. Thus, to leading order,

$$a' = f(a) - 4\pi d_2 a + \frac{4\pi d_2 d_1}{D + d_1}\, a = f(a) - Ma. \tag{12}$$

The interaction terms will be of order $\mathcal{O}(R^1)$, thus we first need to calculate the $\mathcal{O}(R^1)$ interaction of a single cell with the environment. A natural ansatz is to assume

$$u = (\alpha + R\beta)\psi(x)$$

and aim to determine α and β s.t. the BC are satisfied up $\mathcal{O}(R^{-1})$.

The BC in this case read

$$Bu = T_1 + T_2 + T_3 + T_4 \stackrel{!}{=} \frac{d_2 a}{R^2},$$

$$T_1 = \frac{1}{4\pi}\frac{e^{(c^T x - R|c|)/(2D)}}{R^2}\,(\alpha + R\beta), \qquad T_2 = \frac{1}{4\pi}\frac{\left(|c| - \frac{x^T c}{R}\right)\, e^{(c^T x - R|c|)/(2D)}}{2DR}\,(\alpha + R\beta),$$
$$T_3 = \frac{c^T x}{R}\frac{1}{4\pi D}\frac{e^{(c^T x - R|c|)/(2D)}}{R}(\alpha + R\beta), \quad T_4 = \frac{d_1}{R^2}\frac{1}{4\pi D}e^{(c^T x - R|c|)/(2D)}(\alpha + R\beta).$$

We expand T_1 to T_4 to order $\mathcal{O}(R^{-1})$, and find

$$T_1 = R^{-2}\left\{\frac{1}{4\pi}\alpha\right\} + R^{-1}\left\{\frac{1}{4\pi}\beta + \frac{1}{8\pi D}\left(\frac{c^T x}{R} - |c|\right)\alpha\right\} + \mathcal{O}(R^0),$$
$$T_2 = R^{-1}\left\{\frac{1}{8\pi D}\left(|c| - \frac{x^T c}{R}\right)\alpha\right\} + \mathcal{O}(R^0), \qquad T_3 = R^{-1}\left\{\frac{1}{4\pi\, D}\frac{c^T x}{R}\alpha\right\} + \mathcal{O}(R^0),$$
$$T_4 = R^{-2}\left\{\frac{d_1}{4\pi D}\alpha\right\} + R^{-1}\left\{\frac{d_1}{4\pi D}\beta + \frac{d_1}{8\pi D^2}\left(\frac{x^T c}{R} - |c|\right)\alpha\right\} + \mathcal{O}(R^0).$$

Like before, the R^{-2} terms yield $\alpha = Ma$, and the next order reads

$$0 = \frac{1}{4\pi}\quad\left[\beta\left(1 + \frac{d_1}{D}\right) - \frac{\alpha}{D}\frac{d_1|c|}{2D} + \frac{\alpha}{D}\,\left(1 + \frac{d_1}{2D}\right)\,\frac{c^T x}{R}\right]\,R^{-1}, \tag{13}$$

which cannot be satisfied.

Remark A.1 The term involving $c^T x$ yields no $\mathcal{O}(R)$ contribution to the differential equation of a because $\int_{|x|=R} c^T x\, do = 0$. Thus, already at this point we may set $\beta = \dfrac{d_1|c|}{2D(D+d_1)}\alpha$ and calculate the equation for a. Using (11) we obtain

$$a' = f(a) - Ma + R|c|\left(\frac{d_1^2}{2D^2(D+d_1)} - \frac{d_1}{2D^2}\right)\alpha + \mathcal{O}(R^2) = f(a) - M(1 + R\gamma|c|)a + \mathcal{O}(R^2)$$

with $\gamma = \frac{d_1}{2D(D+d_1)}$, cf. (4). ⌋

Remark A.2 In the applications above, $D \approx 5{\cdot}10^{-10}\,\mathrm{m}^2/\mathrm{s}$ and $R \approx 3.6{\cdot}10^{-7}\mathrm{m}$, i.e., parameters have quite different magnitudes also relative to R. Thus, expansions like (11) should be taken with care. For instance, $1 - R|c|/(2D)$ becomes negative for $|c| > |c^*| \approx 0.002778$ m/s. In fact, using spherical coordinates and $\displaystyle\int \sin\vartheta \mathrm{e}^{\delta\cos\vartheta}\mathrm{d}\vartheta = -\frac{1}{\delta}\mathrm{e}^{\delta\cos\vartheta}$ we may as well evaluate

$\int_{|x|=R} \frac{\psi}{R} \mathrm{d}o = \frac{1}{cR}(1 - \mathrm{e}^{-cR/D})$ explicitly, and find that the relative error between $\int_{|x|=R} \frac{\psi}{R} \mathrm{d}o$ and its $\mathcal{O}(R)$ Taylor-expansion exceeds 0.4 for $|c| > |c^*|/2$. For consistency with the Taylor expansions of the boundary conditions as in (10) we stick to the expansion (11), and keep in mind considerations as above when applying the results of the expansions to realistic parameter values. In the simulation in §3 we have $|c_0| = 3.65 \cdot 10^{-4}\mathrm{m/s} \approx |c^*|/8$ and the error in the Taylor expansion is negligible. ⌋

To find a consistent approximation of the outer field we now augment our ansatz. The new ansatz reads

$$u = (\alpha + R\beta)\psi(x) + R^2\theta\ (c^T\nabla\psi)(x). \tag{14}$$

We first work out $\nabla(c^T\nabla\psi(x))$, to find

$$\begin{aligned}
(c^T\nabla\psi)(x) =& \frac{1}{4\pi D}\left(-\frac{c^T x}{|x|^3} + \frac{|c|^2}{2D|x|} - \frac{|c|\,c^T x}{2D|x|^2}\right)\ e^{(c^T x - |x||c|)/(2D)}, \quad \text{hence} \\
\nabla(c^T\nabla\psi)(x) =& \frac{1}{4\pi D}\left(-\frac{c}{|x|^3} + \frac{3\,x\,(c^T x)}{|x|^5} - \frac{|c|^2\,x}{2D|x|^3}\right)\ e^{(c^T x - |x||c|)/(2D)} \\
&+ \frac{1}{4\pi D}\left(-\frac{|c|\,c}{2D|x|^2} + \frac{|c|\,(c^T x)\,x}{D|x|^4}\right)\ e^{(c^T x - |x||c|)/(2D)} \\
&+ \frac{1}{8\pi D^2}\left(-\frac{c^T x}{|x|^3} + \frac{|c|^2}{2D|x|} - \frac{|c|\,c^T x}{2D|x|^2}\right)\left(c - \frac{x|c|}{|x|}\right)\ e^{(c^T x + |x||c|)/(2D)}.
\end{aligned}$$

Thus, with $\nu = -x/R$, and $|x| = R$, we find

$$\begin{aligned}
\nu^T\nabla(c^T\nabla\psi(x)) =& \frac{1}{4\pi\,D}\left(\frac{-2\,c^T x}{R^4} + \frac{|c|^2}{2DR^2} - \frac{|c|\,c^T x}{2DR^3}\right)\ e^{(c^T x - R|c|)/(2D)} \\
&+ \frac{1}{8\pi\,D^2}\left(-\frac{c^T x}{R^3} + \frac{|c|^2}{2DR} - \frac{|c|\,c^T x}{2DR^2}\right)\left(\frac{c^T x}{R} - |c|\right)\ e^{(c^T x + R|c|)/(2D)}.
\end{aligned}$$

Furthermore, $(\nu^T c)(c^T\nabla\psi)(x) = -\frac{1}{4\pi\,D}\frac{c^T x}{R}\left(-\frac{c^T x}{R^3} + \frac{|c|^2}{2DR} - \frac{|c|\,c^T x}{2DR^2}\right)\ e^{(c^T x - |x||c|)/(2D)}$ and therefore

$$R^2 B(c^T\nabla\psi) = R^2\nu^T\left[D\nabla(c^T\nabla\psi) - c(c^T\nabla\psi)\right] + Rd_1(c^T\nabla\psi) = -\frac{1}{4\pi}\left(\frac{2\,c^T x}{R^2} + d_1\frac{c^T x}{R^2}\right) + \mathcal{O}(R^0)$$

Thus, (13) becomes

$$0 = R^{-1}\left[\beta\left(1 + \frac{d_1}{D}\right) - \frac{d_1|c|}{2D^2}\,\alpha\right] + \frac{c^T x}{R^2}\left[\frac{d_1}{2D^2}\alpha - \frac{d_1 + 2D}{D}\theta\right], \tag{15}$$

and β, θ are uniquely determined to

$$\beta = \frac{d_1|c|}{2D(d_1 + D)}\alpha, \qquad \theta = \frac{d_1}{2D(d_1 + 2D)}\alpha. \tag{16}$$

A.2 Several Cells

We localize cells in $x_1 = 0$,.., x_N, and assume

$$u(x) = \sum_{i=1}^{N} \Big[(\alpha_i + R\beta_i)\psi_i(x - x_i) + R^2\theta_i(c^T\nabla\psi)(x - x_i) \Big] \tag{17}$$

In leading order only self-interaction is of relevance, hence again $\alpha_i = Ma_i$. To calculate the interaction terms we focus on the cell located in $x_1 = 0$ and determine "what's coming in". Only the leading order terms of the other cells play a role and thus we determine $B_1\psi(x - x_j)$. For cell one, we again find $\nu = -x/R$, and thus, since $|x - x_j| = \mathcal{O}(|x_j|) = \mathcal{O}(R^0)$,

$$\begin{aligned}(\nu\nabla\psi)(x - x_j) =& -\frac{x^T}{R}\frac{1}{4\pi D}\Big(-\frac{x - x_j}{|x - x_j|^3} + \frac{c}{2D|x - x_j|} - \frac{(x - x_j)|c|}{2D|x - x_j|^2}\Big) e^{(c^T(x-x_j)-|c||x-x_j|)/(2D)} \\ =& \mathcal{O}(R^0),\\ \nu^T c\psi(x - x_j) =& \mathcal{O}(R^0), \qquad \frac{d_1}{R}\psi(x - x_j) = R^{-1}\frac{d_1}{4\pi D}\frac{e^{(c^T x_j-|c||x_j|)/(2D)}}{|x_j|} + \mathcal{O}(R^0).\end{aligned}$$

Therefore, $B_1\psi(x - x_j) = R^{-1}\dfrac{d_1}{4\pi D}\dfrac{e^{(c^T x_j-|c||x_j|)/(2D)}}{|x_j|} + \mathcal{O}(R^0)$, and (15) is modified to

$$0 = \beta_i\left[1+\frac{d_1}{D}\right] + \alpha_i\,\frac{d_1}{2D^2}\,\frac{c^T x}{R} - \alpha_i\,\frac{d_1|c|}{2D^2} - \theta_i\left[2+\frac{d_1}{D}\right]\,\frac{c^T x}{R} + \sum_{j\neq i}\frac{d_1}{D}\frac{e^{(c^T(x_j-x_i)-|c||x_j-x_i|)/(2D)}}{|x_j - x_i|}\alpha_j.$$

Thus, altogether, $\alpha_i = Ma_i$ and

$$\beta_i = \frac{d_1|c|}{2D(D + d_1)}\alpha_i - \sum_{i\neq j}\frac{d_1}{D + d_1}\frac{e^{(c^T(x_j-x_i)-|x_j-x_i||c|)/(2D)}}{|x_j - x_i|}\alpha_j, \qquad \theta_i = \frac{d_1}{2D(d_1 + 2D)}\alpha_i. \tag{18}$$

It remains to derive the ODEs for $a_i, i = 1, \ldots, N$ from $a_i' = f(a_i) - 4\pi a_i + \displaystyle\int_{\partial\Omega_i}\frac{d_1 u}{R}do$. To order $\mathcal{O}(R)$ (where it is easy to see that the terms involving θ_i do not yet contribute) we find

$$a_i' = f(a_i) - 4\pi d_2 a_i + d_1\sum_j I_{ij}, \qquad I_{ij} = (\alpha_j + R\beta_j)\int_{\partial\Omega_i}\frac{\psi(x - x_j)}{R}\mathrm{d}o.$$

Thus, additional to $\displaystyle\int_{\partial\Omega_i}\frac{\psi(x - x_i)}{R}\mathrm{d}o = \frac{1}{D}\big[1 - R|c|/(2D) + \mathcal{O}(R^2)\big]$, cf. (11), we need to evaluate

$$\begin{aligned}\int_{\partial\Omega_i}\frac{\psi(x - x_j)}{R}\,do &= \frac{1}{4\pi D}\int_{\partial\Omega_i}\frac{e^{(c^T(x_i+\mathcal{O}(R)-x_j)-|c||x_i+\mathcal{O}(R)-x_j|)/(2D)}}{R|x_i + \mathcal{O}(R) - x_j|}do \\ &= \frac{1}{D}\,\frac{R}{|x_i - x_j|}\mathrm{e}^{(c^T(x_i-x_j)-|c||x_i-x_j|)/2D} + \mathcal{O}(R^2)\end{aligned}$$

for $i \neq j$. Thus, to $\mathcal{O}(R)$,

$$\begin{aligned}I_{ii} &= (\alpha_i + R\beta_i)\frac{1}{D}\left(1 - \frac{R|c|}{2D}\right) = \frac{1}{D}\alpha_i + \frac{R}{D}(\beta_i - \frac{|c|}{2D}\alpha_i),\\ I_{ij} &= \frac{R}{D|x_i - x_j|}\mathrm{e}^{(c^T(x_i-x_j)-|c||x_i-x_j|)/2D}\alpha_j, \quad i \neq j,\end{aligned}$$

and hence

$$a_i' = f(a_i) - Ma_i + \frac{d_1 R}{D}\left(\beta_i - \frac{|c|}{2D}\alpha_i + \sum_{j\neq i}\frac{\alpha_j}{|x_i - x_j|}\mathrm{e}^{(c^T(x_i-x_j)-|c||x_i-x_j|)/(2D)}\right) \tag{19}$$

where $\alpha_j = Ma_j$ and β_j is given in terms of $(a_1, \ldots, a_N)$ by (18), which yields (3). For $c = 0$ we have $\beta_i = -\frac{d_1}{D+d_1}\sum_{j\neq i}\frac{\alpha_j}{|x_i-x_j|}$, hence

$$\beta_i + \sum_{j\neq i}\frac{\alpha_j}{|x_i - x_j|} = \sum_{j\neq i}\left(1 - \frac{d_1}{d_1 + D}\right)\frac{\alpha_j}{|x_i - x_j|} = \sum_{j\neq i}\frac{D}{d_1 + D}\frac{\alpha_j}{|x_i - x_j|},$$

and thus

$$a_i' = f(a_i) - Ma_i + R\frac{d_1 M}{d_1 + D}\sum_{j\neq i}\frac{a_j}{|x_i - x_j|},$$

which recovers the result of [15, 16].

A.3 Confined space: flow through a tube at spatially independent velocity

In this section we consider a tube of rectangular profile. In order to carry over the arguments from above, we again assume that the flow through the tube is laminar, and the velocity does not depend on the location. In particular, the velocity does not vanish at the walls of the tube. On this surface, bacteria are located that are assumed to have the shape of a half-sphere. These assumptions may be more appropriate if we consider bacterial colonies instead of single bacteria.

To approximate this setup by (3) let us define the scenario more formally. Let $\Omega_{\text{tube}} = \{(x, y, z) : 0 < x, y < L\}$ and $c = (0, 0, 1)^T c_0$ be the tube and the fluid velocity, and let half-spheres with radius R be located at $x_1, \ldots, x_N \in \partial\Omega_{\text{tube}}$. This also means that the cells have distance $> R$ from the tube edges, and necessarily $R < L/2$. We define the region $\Omega = \Omega_{\text{tube}} \setminus \cup_{i=1}^N \{|x - x_i| < R\}$ and split the boundary of Ω into $n + 1$ parts, the wall of the tube itself, and the surface of each half-sphere, $\partial\Omega = \partial\Omega_T \cup \partial\Omega_i$ with

$$\partial\Omega_T = \partial\Omega_{\text{tube}} \setminus \cup_{i=1}^N \{|x - x_i| \leq R\}, \quad \partial\Omega_i = \{|x - x_i| = R\} \cap \Omega_{\text{tube}}.$$

As usual, ν denotes the outer normal of the region Ω. The PDE for the signalling substance reads

$$u_t = D\Delta u + c^T \nabla u, \qquad \partial_\nu u|_{\partial\Omega_T} = 0, \qquad B_i u|_{\partial\Omega_i} = 0$$

where B_i is the boundary value operator introduced in (2b); we furthermore assign for each cell the "internal" function $a_i(t)$, that follows the ODE (2c).

This spatially confined setting can be replaced by a full sphere scenario that fits into the situation considered above by introducing "virtual" spheres in full space. In a first step, we mirror the cells via

$$x_{i,0} = x_i, \qquad x_{i,1} = \mathrm{diag}(-1, 1, 1)x_i, \qquad x_{i,2} = \mathrm{diag}(1, -1, 1)x_i, \qquad x_{i,3} = \mathrm{diag}(-1, -1, 1)x_i$$

where $\mathrm{diag}(a, b, c)$ indicates a diagonal matrix. Next we extend the points periodically in x and y direction,

$$x_{i,j,k,l} = x_{i,l} + j(2\,L, 0, 0)^T + k(0, 2\,L, 0)^T, \qquad i \in \{1, .., N\}, \quad j, k \in \mathbb{Z}, \quad l \in \{0, .., 3\}$$

and re-define $\Omega_{i,j,k,l}$ as full spheres with radius R and centres $x_{i,j,k,l}$. Now we are back to the model given in (2a)-(2c). Symmetry considerations imply that the solution of this surrogate configuration satisfies $\partial_\nu u = 0$ on $\partial\Omega_T$. Also due to symmetry reasons, all locations $x_{i,j,k,l}$ for i

given correspond to a single function $a_i(t)$, independently of j, k and l, and we identify $a_{i,j,k,l} = a_i$. Our formal argument shows, that the solution of this system can be well approximated by (3) and (5), where the sum extends over all sites $x_{i,j,k,l}$. Since we do not include a degradation term for the signalling substance, this infinite sum diverges pointwise if $c = 0$, which is why we used the vanishing small $c = 10^{-10}$ in the simulation in Fig. 4(b1),(c1).

For the simulation of (3) we conveniently truncate to finitely many virtual cells $x_{i,j,k,l}$, $(j,k) \in J \subset \mathbb{Z}^2$. This also removes the divergence of (3), (5) in case $c = 0$, and thus we rather set $c = 10^{-10}$ in the simulations for formal reasons. The system (3) can then be rewritten as

$$a_i' = f(a_i) - M(1 + R\gamma|c|)a_i + R\tilde{M}_i a_i + R\frac{d_1 M}{D + d_1} \sum_{\substack{m=1,\dots,N \\ m\neq i}} I_{im} a_m, \qquad i = 1, \dots, N, \tag{20}$$

where the interaction factor $\tilde{M}$ of a_i with its virtual mirrors and the interaction matrix I_{im} with the other cells can be calculated in advance, namely

$$\tilde{M}_i = \frac{d_1 M}{D + d_1} \sum_{(j,k,l)\in J\times\{0,\dots,3\}} \frac{1}{|x_i - x_{i,j,k,l}|} \exp\left(\frac{c^T(x_i - x_{i,j,k,l}) - |c|\,|x_i - x_{i,j,k,l}|}{2D}\right),$$

$$I_{im} = \sum_{(j,k,l)\in J\times\{0,\dots,3\}} \frac{1}{|x_i - x_{m,j,k,l}|} \exp\left(\frac{c^T(x_i - x_{i,j,k,l}) - |c|\,|x_i - x_{m,j,k,l}|}{2D}\right).$$

In the numerics in Fig. 4 we introduced $2N_0(2N_0{+}3){+}1$ virtual spheres, $x_{i,j,k,l}$, $j = -N_0, \dots, N_0$, $j = -N_0, \dots, N_0{+}1$, $j^2{+}k^2 \neq 0$, $l = 0$, for each original sphere x_i, by assuming that the first two components of each x_i are $y = 0$ and $x = L/2$, and shifting by L, which makes the l–symmetries above redundant. Then $N_0 = 10$ turns out to be more than sufficient to satisfy the boundary conditions $\partial_\nu u|_{\partial\Omega_T}$ with high accuracy.

B The singularity solution

The singularity solution $\psi(x)$ of $0 = D\Delta u - c\nabla u$ resembles the well known Gaussian plume, which is also used to describe the spread of smoke or pollutant plumes originated from a point source [2]; the only difference is that the standard Gaussian plume neglects the diffusion within the drift direction. The singularity solution can be computed via

$$u_t = D\Delta u - c\nabla u + \delta_0, \quad u|_{t=0} = u_0 \quad \Leftrightarrow \quad u(t,x) = T_t u_0 + \int_0^t T_{t-s}\delta_0\, ds$$

and taking $\lim_{t\to\infty} u(t,x)$, where $T_t f = \displaystyle\int_{\mathbb{R}^3} \frac{e^{-|x-ct-x'|^2/(4Dt)}}{(4\pi Dt)^{n/2}} f(x')\, dx'$. Thus,

$$\begin{aligned}\psi(x) &= \int_0^\infty \frac{e^{-|x-ct|^2/(4Dt)}}{(4\pi Dt)^{n/2}}\, dt = (4\pi D)^{-n/2} \int_0^\infty \exp\left\{-\frac{1}{4D}\left(\frac{|x|^2}{t} - 2c^T x + |c|^2 t\right)\right\} t^{-n/2}\, dt \\ &= (4\pi D)^{-n/2} e^{c^T x/(2D)} \int_0^\infty \exp\left\{-\frac{1}{4D}\left(\frac{|x|^2}{t} + |c|^2 t\right)\right\} t^{-n/2}\, dt.\end{aligned}$$

As this integral is somewhat less standard than the Gauss integral $\int_0^\infty (4\pi t)^{-n/2} \mathrm{e}^{-|x|^2/(4Dt)} \mathrm{d}t = 1/\|x\|$ for $n = 3$, we now give the calculations to evaluate it explicitly. With $w = |x|^2/(4Dt)$ we

find

$$\begin{aligned}\psi(x) =&(4\pi D)^{-n/2} e^{c^T x/(2D)} \left(\frac{|x|^2}{4D}\right)^{-n/2+1} \int_0^\infty w^{n/2-2}\, e^{-w}\, e^{-\frac{|c|^2|x|^2}{(4D)^2\, w}}\, dw \\ =&\frac{\pi^{-n/2}}{4D} e^{c^T x/(2D)} |x|^{2-n} \int_0^\infty w^{n/2-2}\, e^{-w}\; e^{-\frac{|c|^2|x|^2}{(4D)^2\, w}}\, dw\end{aligned}$$

Next define $h^2 = |c|^2|x|^2/(4D)^2$ and $I_\alpha(h) = \int_0^\infty w^{\alpha/2-2} e^{-w-h^2/w}\, dw$.

Lemma B.1 *$I_3(h) = \sqrt{\pi} e^{-2h}$ and thus $\psi(x) = \dfrac{1}{4\pi\, D} \dfrac{e^{(c^T x - |x||c|)/(2D)}}{|x|}$.*

Proof. The function $\zeta(w) = w/2 + h^2/(2w)$ is monotonous in $[0, h)$ and in (h, ∞), where $\zeta(h) = h$. With $w = w(\zeta) = \zeta \pm \sqrt{\zeta^2 - h^2}$ and $w'(\zeta) = 1 \pm \zeta/\sqrt{\zeta^2 - h^2} = (\sqrt{\zeta^2 - h^2} \pm \zeta)/\sqrt{\zeta^2 - h^2}$ we obtain

$$\begin{aligned}I_\alpha(h) &= \int_0^\infty w^{\alpha/2-2}\, e^{-w-h^2/w}\, dw \\ &= \int_\infty^h (\zeta - \sqrt{\zeta^2 - h^2})^{\alpha/2-2} \frac{\sqrt{\zeta^2 - h^2} - \zeta}{\sqrt{\zeta^2 - h^2}} e^{-2\zeta}\, d\zeta + \int_h^\infty (\zeta + \sqrt{\zeta^2 - h^2})^{\alpha/2-2} \frac{\sqrt{\zeta^2 - h^2} + \zeta}{\sqrt{\zeta^2 - h^2}} e^{-2\zeta}\, d\zeta \\ &= \int_h^\infty \frac{(\zeta - \sqrt{\zeta^2 - h^2})^{\alpha/2-1} + (\zeta + \sqrt{\zeta^2 - h^2})^{\alpha/2-1}}{\sqrt{\zeta^2 - h^2}}\; e^{-2\zeta}\, d\zeta.\end{aligned}$$

Fix $\alpha = 3$. Then $\alpha/2 - 1 = 1/2$,

$$\begin{aligned}&\left((\zeta - \sqrt{\zeta^2 - h^2})^{1/2} + (\zeta + \sqrt{\zeta^2 - h^2})^{1/2}\right)^2 \\ &\qquad = \zeta - \sqrt{\zeta^2 - h^2} + 2\left(\zeta^2 - (\zeta^2 - h^2)\right)^{1/2} + \zeta + \sqrt{\zeta^2 - h^2} = 2(\zeta + h), \quad (21)\end{aligned}$$

and $I_3(h) = \int_h^\infty \frac{\sqrt{2}(\zeta+h)^{1/2}}{\sqrt{\zeta^2-h^2}} e^{-2\zeta}\, d\zeta = \int_h^\infty \frac{\sqrt{2}}{\sqrt{\zeta - h}} e^{-2\zeta}\, d\zeta = \int_0^\infty \frac{\sqrt{2}}{\sqrt{\eta}} e^{-2\eta}\, d\eta e^{-2h} = \Gamma(1/2) e^{-2h} = \sqrt{\pi} e^{-2h}$. □

References

[1] E. Alpkvist, C. Picioreanu, M. van Loosdrecht, and A. Heyden. Three-dimensional biofilm model with individual cells and continuum EPS matrix. *Biotech. and Bioeng.*, 94:961–979, 2001.

[2] N. Arystanbekova. Application of gaussian plume models for air pollution simulation at instantaneous emissions. *Math. Comp. Simul.*, 67:451–458, 2004.

[3] J. Chuang, O. Rivoire, and S. Leibler. Simpson's paradox in a synthetic microbial system. *Science*, 323:272–275, 2009.

[4] T. Czárán and R. Hoekstra. Microbial communication, cooperation and cheating: Quorum sensing drives the evolution of cooperation in bacteria. *PLoS ONE*, 4:e6655, 1–9, 2009.

[5] J. Dockery and J. Keener. A mathematical model for quorum sensing in *pseudomonas aeruginosa*. *Bull. Math. Biol.*, 63:95–116, 2001.

[6] H. Eberl, E. Morgenroth, and D. Noguera. *Mathematical Modeling of Biofilms*. Iwa Publishing, 2006.

[7] A. Fekete, C. Kuttler, M. Rothballer, D. Fischer, K. Buddrus-Schiemann, B. Hense, M. Lucio, J. Müller, P. Schmitt-Kopplin, and A. Hartmann. Dynamic regulation of n-acyl-homoserine lactone production and degradation in pseudomonas putida isof. *FEMS Microb. Ecol.*, 62:22–34, 2010.

[8] M. Frederick, C. Kuttler, B. Hense, J. Müller, and H. Eberl. A mathematical model of quorum sensing in patchy biofilm communities with slow background flow. *Canad. Appl. Math. Quart.*, 18:267–298, 2010.

[9] A. Goryachev, D.-J. Toh, K. Wee, T. Lee, and H.-B. Zhang. Transition to quorum sensing in an agrobacterium population: A stochastic model. *PLoS Comput. Biol.*, 1:e37, 2005, DOI: 10.1371/journal.pcbi.0010037.

[10] J. Harrison, R. Turner, L. Marques, and H. Ceri. A new understanding of these microbial communities is driving a revolution that may transform the science of microbiology. *Am. Sci.*, 93:508–515, 2005.

[11] B. Hense, C. Kuttler, J. Müller, M. Rothballer, A. Hartmann, and J.-U. Kreft. Does efficiency sensing unify diffusion and quorum sensing? *Nat. Rev. Microbiol.*, 5:230–239, 2007.

[12] A. Horswill, P. Stoodley, P. Stewart, and M. Parsek. The effect of the chemical, biological, and physical environment on quorum sensing in structured microbial communities. *Anal. Bioanal. Chem.*, 287:371–380, 2007.

[13] H. Kaplan and E. Greenberg. Diffusion of autoinducer is involved in regulation of the vibrio fischeri luminescence system. *J. Bacteriol.*, 163:1210–1214, 1985.

[14] A. Meyer, J. Megerle, C. Kuttler, J. Müller, C. Aguilar, L. Eberl, B. Hense, and J. Rädler. Dynamics of AHL mediated quorum sensing under flow and non-flow conditions. *Phys. Biol.*, 9:026007 (10pp), 2012.

[15] J. Müller, C. Kuttler, B. Hense, M. Rothballer, and A. Hartmann. Cell-cell communication by quorum sensing and dimension-reduction. *J. Math. Biol.*, 53:0672–702, 2006.

[16] J. Müller and H. Uecker. Approximating the dynamics of communicating cells in a diffusive medium by ODEs – Homogenization with Localization. *J. Math. Biol.*, 53:0672–702, 2012, DOI: *10.1007/s00285-012-0569-y*.

[17] B. Purevdorj, J. Costerton, and P. Stoodley. Influence of hydrodynamics and cell signaling on the structure and behavior of *pseudomonas aeruginosa* biofilms. *Appl. Envir. Microb.*, 68:4457–4464, 2002.

[18] R. Redfield. Is quorum sensing a side effect of diffusion sensing? *Trends Microbiol.*, 10:365–370, 2002.

[19] M. Schuster, D. Sexton, S. Diggle, and E. Greenberg. Acyl-homoserine lactone quorum sensing: From evolution to application. *Ann. Rev. Microbiol.*, page submitted, 2013.

[20] P. Steward. Diffusion in biofilms. *J. Bacteriol.*, 185:1485–1491, 2003.

[21] B. Vaughan, B. Smith, and D. Chopp. The influence of fluid flow on modeling quorum sensing in bacterial biofilms. *Bull. Math. Biol.*, 72:1143–1165, 2010.

[22] N. Wai-Leung and B. Bassler. Bacterial quorum-sensing network architectures. *Annu. Rev. Genet.*, 43:197–222, 2009.

[23] P. Williams, K. Winzer, W. Chan, and M. Camara. Look who's talking: communication and quorum sensing in the bacterial world. *Phil. Trans. R. Soc. B*, 362:1119–1134, 2007.